Nanoscale Origins of Nonlinear Behavior in Ferroic Thin Films

Rama K. Vasudevan, M. Baris Okatan, Chen Duan, Yoshitaka Ehara, Hiroshi Funakubo, Amit Kumar, Stephen Jesse, Long-Qing Chen, Sergei V. Kalinin, and Valanoor Nagarajan**

The nonlinear response of a ferroic to an applied field has been studied through the phenomenological Rayleigh Law for over a hundred years. Yet, despite this, the fundamental physical mechanisms at the nanoscale that lead to macroscopic Rayleigh behavior have remained largely elusive, and experimental evidence at small length scales is limited. Here, it is shown using a combination of scanning probe techniques and phase field modeling, that nanoscale piezoelectric response in prototypical $Pb(Zr,Ti)O_3$ films appears to follow a distinctly non-Rayleigh regime. Through statistical analysis, it is found that an averaging of local responses can lead directly to Rayleigh-like behavior of the strain on a macroscale. Phase-field modeling confirms the twist of the ferroelastic interface is key in enhancing piezoelectric response. The studies shed light on the nanoscale origins of nonlinear behavior in disordered ferroics.

1. Introduction

The nonlinear response of a ferroic to an applied stimulus (e.g., electric field, mechanical stress) is a fundamental characteristic that underpins a number of technologically significant applications.[1,2,3] It is also the driving feature in numerous physical phenomena, such as interfacial motion,[4,5] spin glasses,[6] relaxors[7] and phase transitions.[8] In particular, nonlinearity associated with minor hysteresis loops is an extremely useful avenue to explore energy dissipation and losses in such systems. This knowledge is necessary for the design of future materials with enhanced low-field properties. Quantitatively, the macroscopic nonlinear response of ferroic systems at low to mid-range amplitudes of driving fields is given by the phenomenological Rayleigh law,[9] first conceived in 1887 for magnetic materials. Yet, the applicability of the Rayleigh law at small length scales has not been extensively studied.

The first major attempt to produce a physical model to explain Rayleigh's law of weak-field magnetic hysteresis was provided by Néel in the 1940s.[10] In his seminal paper, Néel assumed the problem of the motion of a domain wall through a medium with random defect distribution under weak field excitation, and found that such behavior results in magnetization that is well described by the Rayleigh law. In its general form, the Rayleigh law states that there is a linear dependence of the susceptibility on the applied field, and that this dependence arises from small, irreversible domain wall motions resulting in hysteretic response.[11] However, such an analysis may no longer hold valid where the spatial distribution of variation in the pinning potential is of the same order as the displacements of the propagating interface, and therefore suggests an inherent size limit for observing Rayleigh behavior. For example, scanning probe-based studies on ferroelectric thin films by Shvartsman et al. indicated that the piezoelectric coefficient may not be field-dependent at the nanoscale.[12] From a theoretical perspective, efforts have ranged from the mechanisms mediated by dynamics of a single wall in the presence of static or moving pinning centers[13–19] to the nature of the order parameter that characterizes the domain wall.[20–22] Recent experimental studies have also highlighted the key role of collective domain wall interactions,[23] as well as the Rayleigh-like behavior of non-180° domain wall motion,[24] in contributing to nonlinear behavior.[25,26] Studies on ferroelectric thin-films have also shown that even the mostly-reversible motion of any interface ("dynamic poling") can result in a Rayleigh-like behavior of the strain.[27–29] Yet, despite 125 years since the Rayleigh law was conceived, a clear picture of the behavior at the nanoscale is yet to emerge, and in particular, the degree of enhancement in the response from interfacial motion at such length scales has not been well characterized experimentally.

R. K. Vasudevan, Dr. M. B. Okatan, Prof. V. Nagarajan
University of New South Wales
Kensington, 2052, Australia
E-mail: nagarajan@unsw.edu.au
C. Duan, Prof. L. Q. Chen
Department of Materials Science and Engineering
Pennsylvania State University
University Park, PA 16802, USA
Y. Ehara, Prof. H. Funakubo
Department of Innovative Engineered Materials
Tokyo Institute of Technology, 4259 Nagatsuta
Midori-ku, Yokohama, 226-8502, Japan
Dr. A. Kumar, Dr. S. Jesse, Prof. S. V. Kalinin
The Center for Nanophase Materials Sciences
Oak Ridge National Laboratory
Oak Ridge, TN 37831, USA
E-mail: sergei2@ornl.gov

DOI: 10.1002/adfm.201201025

In this report we use advanced band-excitation scanning probe techniques[30] alongside phase-field simulations to reveal the nanoscale origins of nonlinear behavior in ferroelectric thin-films at the single-domain level. The band-excitation probes allow direct imaging and measurement of piezoresponse at individual domain walls, and overcome inherent resolution limits that have stymied experimental approaches to date. We note here that the term "piezoresponse" hereafter refers to the local bias-induced strain generated through the converse piezoelectric effect, resulting from applying a probing AC voltage (V_{ac}) to the cantilever tip. We find that the piezoresponse is heavily position-dependent, and often does not follow the expected Rayleigh regime[31] observed for meso- and macro-scale probed volumes of ferroelectrics. Additionally, the activated motion of ferroelastic walls, initiated at a critical energy level (in our case critical voltage V_c) is a source of significant deviation from linear intrinsic material response. In contrast, experimental studies and modeling of a single ferroelectric (180°) wall show no enhancement in the piezoresponse from wall motion. Deconstructing the piezoresponse curves at individual points (i.e., local measurements) indicates that piezoresponse for the case of ferroelastic domains appears to follow a two linear segments (TLS) model, with the gradient of the second segment ($V_{ac} > V_c$) generally higher than the gradient of the first ($V_{ac} < V_c$). The increased gradient in the second segment is ascribed to the onset of a wall motion, comprising the extrinsic response whose amplitude is found to exhibit a linear dependence on V_{ac} up to the maximum amplitude of the probing voltage applied. Phase-field modeling confirms the crucial role of the twist of the ferroelastic interface in enhancing the local piezoresponse. Through an averaging approach, it is shown that a distribution in V_c and other response parameters leads directly to a type of nonlinearity in piezoresponse on the macroscale, and results in the observed linear dependence of the effective piezoelectric coefficient on the applied bias, consistent with the Rayleigh law. Hence, collective responses from individual non-Rayleigh-like activated motion of ferroelastic walls at the nanoscale can lead directly to Rayleigh-like behavior as an assemblage on larger scales.

2. Results and Discussion

To explore the nanoscale origins of Rayleigh behavior, we choose films of the widely studied prototypical ferroelectric $Pb(Zr,Ti)O_3$ (PZT) as a model system. This choice offers numerous advantages: imaging of the domain structures on films, with nanometer precision is relatively common with commercially available piezoresponse force microscopy setups. Moreover, PZT films provide a tunable mix (through strain-engineering[32]) of ferroelectric and ferroelastic walls at which the piezoelectric response can be investigated. Since the domain period (and therefore the length scale of the elastic interactions) can also be controlled by varying the film thickness, the response of a single wall, as well as a collective response in an array of domains, can be studied. To decouple the possible contributions, and explore the interplay between single-wall and collective response, three samples of were examined: 1) 2 μm-thick PZT, 2) 200 nm-thick PZT films exhibiting a/c domain structure, and 3) 200 nm-thick *c*-axis-only PZT film containing purely ferroelectric (180°) walls.

The band-excitation method was used to determine the response of the films across an AC bias range, at individual points within a pre-defined grid. The field-dependent piezoresponse of the 2 μm PZT film was investigated first. The domain structure, as explored using PFM, is complex and consists of an array of *a*- and *c*-domains, as evidenced by the lateral PFM amplitude image in **Figure 1**a. Based on lateral and vertical PFM data captured, a polarization map of the region was produced, which is shown in Figure 1b. In this map, it can be seen that there exists predominantly ferroelastic walls (marked in red); however, 180° ferroelectric walls (green) and other more complex a/a domain walls also exist (blue). Note that we have assumed head-to-tail polarization alignments in assigning the polarization directions, and determined the tilt of the a domains by examining the vertical PFM image.[33] It is important to note that the walls are not straight, i.e. there exists a complex structure underneath the surface. Thus, this serves as a platform in which the effects of collective interactions can be explored, as the domain period is on par with the probed volume, i.e., the probed region ($\approx 10^4$ nm^3)[34] is likely to consist of at least one, and in many cases several, domain walls.

The average piezoresponse loop for the region enclosed in the white square shown in Figure 1a is graphed in Figure 1c, and was obtained by the band-excitation PFM method. The average piezoresponse loop displays a sharp change at applied voltages of $V = 0$ V (forward, lower branch) and $V = -3$ V (reverse, upper branch). Nonlinear macroscopic d_{33} hysteresis measurements (captured on a 50 μm in diameter top electrode) are shown in Figure 1d, and confirm that the film displays large electromechanical response.[35,36] X-ray diffraction data (Supporting Information S1) suggests that the cause of the large piezoresponse in this film is ferroelastic switching, which is confirmed by increase in the c-domain fraction of the film (from 24% to 42%) after one switching cycle. Importantly, the macroscopic d_{33} hysteresis loops also shows sharp features in the sub-coercive range, similar to the average piezoresponse hysteresis; therefore, this suggests that these experiments are indeed probing the local analog of the macroscopic properties.

The (vertical) piezoresponse was captured in the boxed square drawn in Figure 1a, by dividing the area into a 70×70 grid and using the PFM tip as a probe to measure the (BE-) piezoresponse (i.e., the PFM tip is itself the electrode) as a function of AC bias. Care was taken to ensure that the choice of excitation function was such that cantilever nonlinearities were kept to a minimum (Supporting Information S2).[37]

Based on the data captured, we were able to discern three different types of behaviors (i.e., dependencies of the piezoresponse on V_{ac}) within this region, which are indicated as three separate colors in the fitting plot in **Figure 2**a. (Statistical details are provided in Supporting Information S3). In this plot, blue, green and red dots, respectively, mark points where piezoresponse at that particular grid-point shows linear, quadratic and "two-linear segment" (TLS) type behaviors. Points where no fit was possible, due to low and/or scattered signals are left empty (i.e., white). These largely stem from the very low piezoresponse found in the a-domains. Examples of the different types of behaviors observed are plotted in Figure 2b.

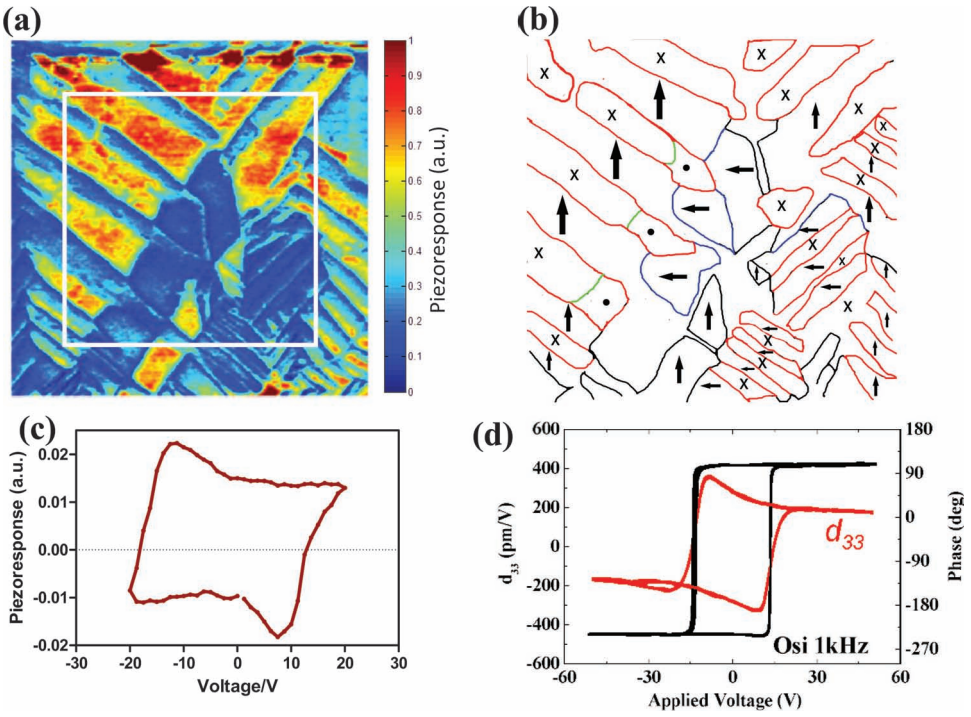

Figure 1. Domain structure and switching experiments of thick PZT sample. a) 1 μm × 1 μm lateral PFM amplitude image of the 2 μm-thick PZT sample, showing large, complex a/c domain structures. A nonlinear study in the white boxed region in (a) was performed. By combining lateral and vertical PFM images, a vector PFM map of the region studied was produced, shown in (b). c) Average piezoresponse loop from the white boxed region in (a), showing distinct hill-like features. Macroscopic phase (black) and d_{33} (red) response as a function of applied bias is shown in (d), as measured by direct PFM.

From the fitting plot, it is clear that in general, the TLS behavior is predominant in areas where the data were reliable. The piezoresponse (P) at each of these points can be characterized by a piecewise function:

$$P(V_{ac}) = \begin{cases} \alpha_1 V_{ac} + c_1, & V_{ac} < V_c \\ \alpha_2 V_{ac} + c_2, & V_{ac} > V_c \end{cases} \quad (1)$$

where V_c is the critical (transition) bias. The fact that TLS behavior is commonly observed at these length scales points to the conclusion that the piezoresponse does not tend to follow the traditional Rayleigh regime, in which it is expected to exhibit a quadratic dependency on V_{ac}, i.e., resulting in a piezoelectric coefficient that would be a linear function of V_{ac}.

The defining feature of the TLS behavior observed is the ratio of the two slopes, i.e., α_2/α_1. We posit that the initial linear region, $V_{ac} < V_c$, is defined by reversible intrinsic (lattice) response (and, if any, reversible contributions due to domain wall vibrations as well), after which the activation energy for irreversible domain wall motion (the transition bias, V_c) is reached, and extra contributions from the wall motion arise. We note here that while it may be possible that the second linear region corresponds to the activation of reversible domain wall motion, the fields applied by the tip are relatively large (≈1 kV mm^{-1} for the 2 μm film as a first approximation), and, combined with minor loop data (unpublished) at voltage ranges ±2.5 V that shows hysteresis, suggest irreversible processes can easily be activated at the voltages used in this study. The transition bias V_c is therefore an indication of the degree of pinning of the domain wall, by either substrate, defects[11] or surrounding domains. Thus, the α_1 is a measure of the intrinsic response, and α_2 is a measure of the intrinsic response plus the additional contribution from domain wall motion at that grid point. Since both α_1 and α_2 vary spatially, then computing the degree of extrinsic response relative to the intrinsic (lattice) response requires mapping the α_2/α_1 ratio. Points where there is no extrinsic contribution, i.e., domain wall movement is severely hindered and thus absence of a transition bias V_c, results in the linear response shown in Figure 2b, while points where the α_2/α_1 is distinctly high should correspond to areas where the relative contribution of domain wall motion to the piezoresponse is significant (dominant). The α_2/α_1 map is shown in Figure 2c. Here, it is readily apparent that this ratio peaks at the domain boundaries, which would be consistent with ferroelastic wall motion as being the source of the increased piezoresponse above the critical bias V_c.

To observe the various fitting parameters as a function of distance to the ferroelastic wall, we consider the c-domains indicated by dashed lines in Figure 2c. Data and schematics pertaining to this region are displayed in Figure 2d–g. In Figure 2d, the α_2/α_1 ratio is plotted on the y-axis, while the domain schematic indicating the a/c domains structure in the same region is shown above the 3D scatter plot in Figure 2e. Taken together, it is evident that as the ferroelastic walls are approached, there is significant peaking in the α_2/α_1 ratio. Within the middle of the c-domains, the ratio is ≈2–4. Since the domain walls in this sample are tilted, and the tip is of finite radius, this behavior at

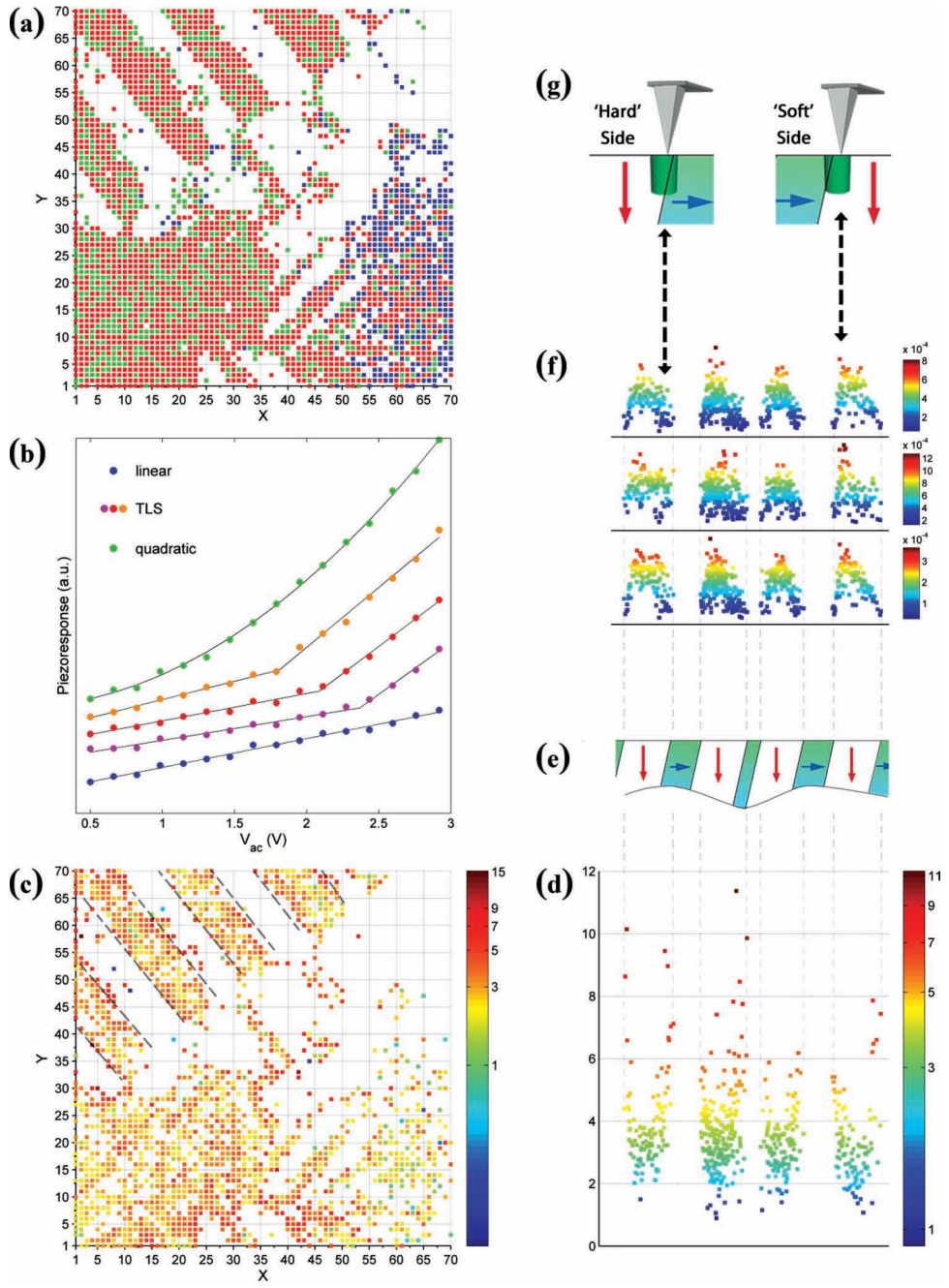

Figure 2. 2 µm-thick PZT sample piezoresponse analysis. a) Fitting map for acquired nonlinear data in 700 nm × 700 nm area marked by white outline in Figure 1a. Regions where the response was best modeled with a TLS fit are marked in red, while regions displaying linear response are marked in blue. Regions displaying quadratic behavior are green. Finally, areas where no fit was possible (due to poor signal) are empty. Of the 2899 grid points, 13% are linear, 26% are quadratic, and 61% are TLS. Examples of these types of behaviors are shown in the five individual response plots (shifted vertically for clarity) in (b). A plot of the α_2/α_1 ratio for the studied region is plotted in (c). Shown in the right hand column is a panel figure (d–g) composed of data and schematics concerning the c-domains outlined (dashed lines) in (c). A plot of the α_2/α_1 ratio in this region is displayed in (d). A schematic of the underlying domain structure, complete with the wall tilts, is indicated in the side-on view in (e). α_1, α_2, and $P(V_c)$ of the four c-domains from this perspective are plotted in (f), from bottom to top, respectively. Depicted in (g) is a schematic of 'hard' and 'soft' sides of the c-domains.

the centre of the c-domains could be due to peripheral contributions from the motion of nearby ferroelastic walls.

To analyze the relationship of the domain wall to the response of the system further, we plot α_1, α_2 and piezoresponse at the critical voltage, $P(V_c)$, for the same region in Figure 2f. These plots show that all three parameters appear to peak close to the left edge of the c-domains, and are lower on the right hand side of the c-domains. This is most likely due to the tilted nature

of the a/c domain walls, which results in two regions within the c-domain, labeled "soft" and "hard", as indicated in the schematic in Figure 2g. The peaking of the parameters at the soft region highlights the crucial role of tilt of the ferroelastic wall in determining the final piezoresponse: when the wall is in close proximity, but where there remains a very significant fraction of c-domains in the probed volume, the response peaks. On the other hand, when the tip is near the hard region of the c-domain, the c-domain within the probed volume is effectively more clamped. These factors lead to asymmetric response across the c-domains, and highlight the crucial role of the presence and tilt of the ferroelastic wall in determining the final piezoresponse. We note here that similar asymmetry was found in the out-of-plane strain within *c*-domains across a *c*/*a*/*c* domain boundary in a lead titanate film by Catalan et al., using scanning transmission electron microscopy.[38]

At the same time, we note here the smaller but not insignificant number of points that are green in Figure 2a, which correspond to piezoresponse with a quadratic dependence on V_{ac}. This could be due to contributions from multiple domain walls in the probed volume. To determine whether this is the case, we carried out the same experiment on a PZT sample of same composition but with a thickness of 200 nm. This sample has a significantly lower domain density, and hence reduces the number of walls in the probed volume. The domain structure is shown in the vertical PFM amplitude image in **Figure 3**a, and exhibits the typical cross-hatch pattern[33] with thin *a*-domains embedded within a largely c-domain matrix. The AC dependent piezoresponse was studied using an AC sweep voltage range of 0.1 to 4.92 V_{ac} at each point in a 100 × 100 grid in this region. The fitting map for this film is shown in Figure 3b. Almost 80% of points exhibit TLS behavior, as indicated by the red points, lending support to the idea that the reason for quadratic behavior at some points in the thicker PZT film is likely due to the collective motion of multiple domain walls in the probed tip-volume, because the main difference between the two samples (which are of same composition) is the density of domain walls.

The α_2/α_1 ratio map for the 200nm-thick PZT film is shown in Figure 3c. Again, it is apparent that the ratio tends to increase near the a/c domain walls; this would be consistent with ferroelastic wall motion as the source of enhanced piezoresponse. On the other hand, the ratio is somewhat smaller than in the 2 μm-thick film. Presumably, this is due to increased clamping of the ferroelastic walls by the substrate. In the case of the thicker 2 μm film, the degree of clamping is determined only by the surrounding domain architecture as opposed to substrate effects, and therefore likely to contain more labile ferroelastic walls. The extent to which the substrate clamping influences the TLS response parameters is a subject of future studies.

To determine the role of substrate-induced strain on the mobility of the ferroelastic domain walls, the transition bias V_c, for both 2 μm- and 200 nm-thick PZT films was inspected, and is shown in the histogram in **Figure 4**a. The transition bias is significantly higher for the thinner film, with a peak at ≈3.8 V, as opposed to ≈2.0 V for the 2 μm-thick PZT film, again highlighting the increased clamping of the ferroelastic walls in the thin film (spatial maps and histograms of V_c along with α_1, α_2 etc. for samples studied are provided in Supporting Information S4).

To ascertain the link between the microscopic and macroscopic (i.e., average of all individual responses) piezoelectric behaviors, we plot the average responses from the three different types of responses in the 2 μm-thick PZT in Figure 4b. The average response of the points exhibiting TLS, quadratic and linear behavior is plotted, respectively, in red, green and blue. The overall average of the entire studied region (excluding white colored regions in Figure 2a) is graphed as a solid black line. Although the quadratic behavior is associated with only 26% of all the points shown, the overall average piezoresponse is best represented by a quadratic behavior. In this case, such a quadratic response for overall average piezoresponse arises due to a spread of TLS responses at individual points resulting in an average TLS response with a broad, diffuse transition region. To investigate this further, we calculated the average response that would be expected from a collection of TLS behaviors, as a function of voltage. The formulation of this calculation is given in Supporting Information S5. Accordingly, calculations indicate that due to a distribution in the critical bias V_c, the resulting average behavior will be a significantly smoother curve than in the microscopic response. Furthermore, this simple approach indicates how macroscopic nonlinear behavior with quadratic dependence on probing voltage can stem from activated, individual domain wall motions–the only necessity is a distribution of behaviors, which can be expected for any real sample (e.g., due to presence of defects, spatially inhomogeneous strain fields,[38] etc.).

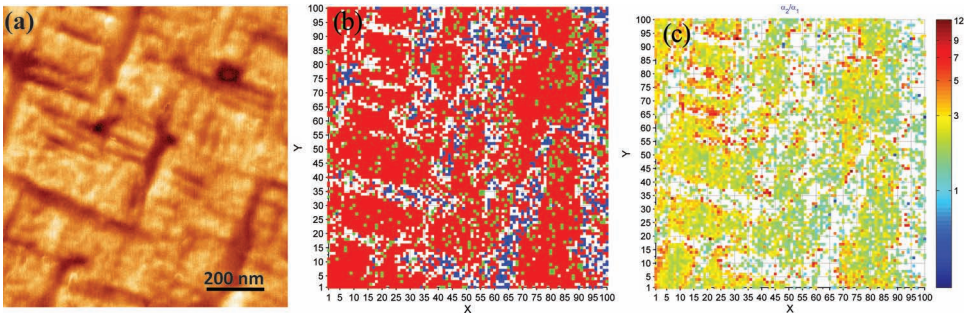

Figure 3. Study of 200 nm-thick PZT sample. a) Vertical PFM amplitude image, showing the typical cross-hatch pattern. b) Fitting map, with the same color scheme as in Figure 2a. Of the 8080 grid points, 10.8% are linear, 9.6% are quadratic, and 79.6% are TLS. TLS behavior is the most commonly observed response. c) α_2/α_1 ratio spatial map for the same region. Again, the peaking of the ratio at the a/c domain boundaries is evident.

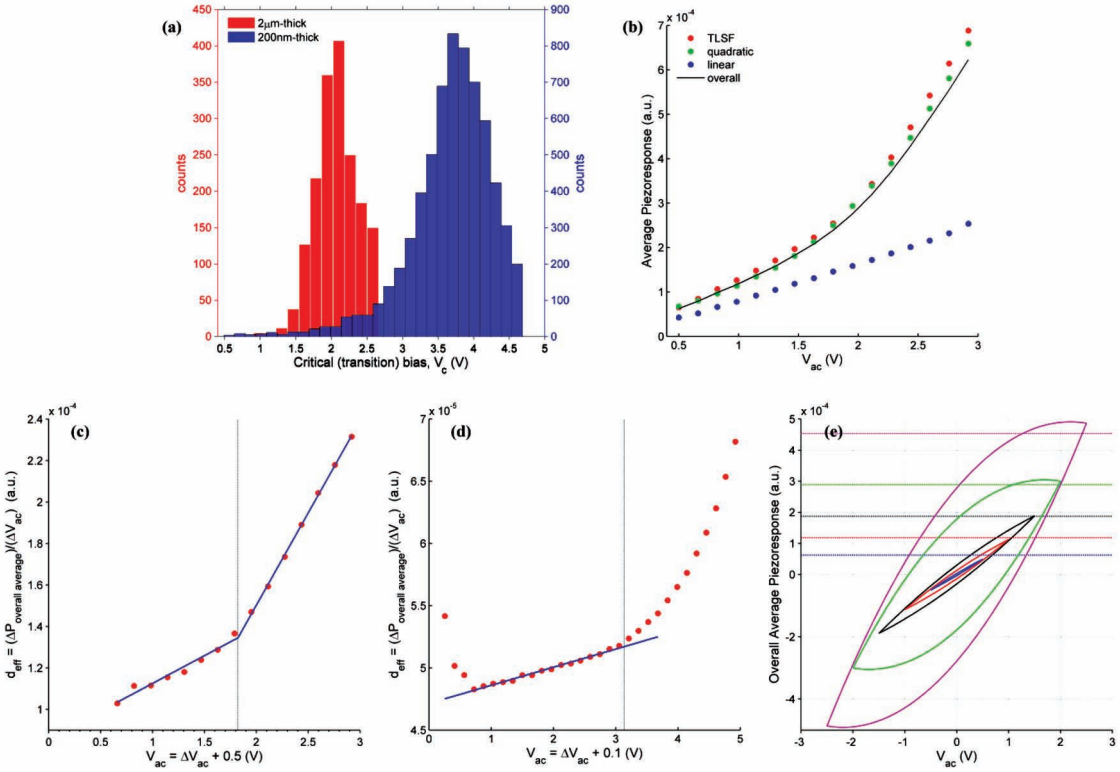

Figure 4. Distributions in individual response can lead to Rayleigh behavior. a) Histograms for the transition voltage V_c for the 2 μm- and 200 nm-thick PZT films. The presence of a distribution in the transition bias leads directly to a nonlinear behavior at the macroscale. The average piezoresponse from regions displaying TLS, quadratic, and linear responses are shown in (b) for the 2 μm thick film. The overall average of all studied points shown in Figure 2a is plotted as a solid line for comparison. c,d) Dependence of d_{eff} on V_{ac}, respectively, for 2 μm- and 200 nm-thick PZT films. e) The expected hysteresis loops for the 2 μm-thick PZT film along with their corresponding P_{ave} values (horizontal dotted lines) from Figure 4b given bottom to top, respectively, for a series of $V^{max}{}_{ac}$: 0.5, 1, 1.5, 2 and 2.5 V.

To determine how local response can lead to Rayleigh behavior on larger length scales, we calculate the effective piezoelectric coefficient d_{eff} as,

$$d_{eff} = \frac{\Delta P}{\Delta V_{ac}} = \frac{P(V_{ac}) - P(V_r)}{V_{ac} - V_r} \quad (2)$$

where ΔP and ΔV_{ac} are, respectively, the change in the overall average piezoresponse and AC probing voltage from the reference condition $(P(V_r), V_r)$. Minimum probing AC voltage was chosen as the V_r, i.e., $V_r = 0.5$ V and 0.1 V for 2 μm- and 200 nm-thick PZT films, respectively. The underlying notion is that the second linear region of the TLS model arises from irreversible (rather than reversible) domain wall motions. Analogous to the electric/stress field dependent variation of the converse/direct piezoelectric coefficient,[11,24] the Rayleigh law in our case for the evolution of d_{eff} with V_{ac} can be written as

$$d_{eff} = d_0 + \alpha_d V_{ac} \quad (3)$$

where d_0 and α_d are the initial d_{eff} at $V_{ac} = 0$ and the Rayleigh coefficient for d_{eff}, respectively. d_0 and $\alpha_d V_{ac}$ represent, respectively, the contributions from reversible and irreversible piezoelectric mechanisms to d_{eff} separately. The variation of d_{eff} for 2 μm- and 200 nm-thick PZT films are shown in Figure 4c,d, respectively. It can be clearly seen that the 2 μm-thick PZT film obeys the Rayleigh law throughout the V_{ac} range studied but surprisingly with two distinct Rayleigh behaviors becoming apparent with respect to a Rayleigh transition voltage, $V_{RT} \approx 1.8$ V whereas the 200 nm-thick PZT film exhibits only one Rayleigh behavior up to $V_{ac} \approx 3.1$ V above which variation of d_{eff} follows a non-Rayleigh-like behavior. It is worth of noting here that such nuances from the regular Rayleigh behavior is due to non-uniformly distributed V_c values, Figure 4a, whereas if the distribution of V_c values was uniform then it would be possible to maintain the regular Rayleigh behavior over the whole range of probing voltages investigated. The Rayleigh behavior of the films are given as

i) 2 μm-thick PZT film

$$d_{eff} = 8.579 \times 10^{-5} + 2.673 \times 10^{-5} \times V_{ac}\ 1^{st}\ \text{Rayleigh region}(V_{ac} < V_{RT} \approx 1.8\text{V}) \quad (4)$$

$$d_{eff} = -2.782 \times 10^{-5} + 8.9 \times 10^{-5} \times V_{ac}\ 2^{nd}\ \text{Rayleigh region}(V_{ac} > V_{RT} \approx 1.8\text{V}) \quad (5)$$

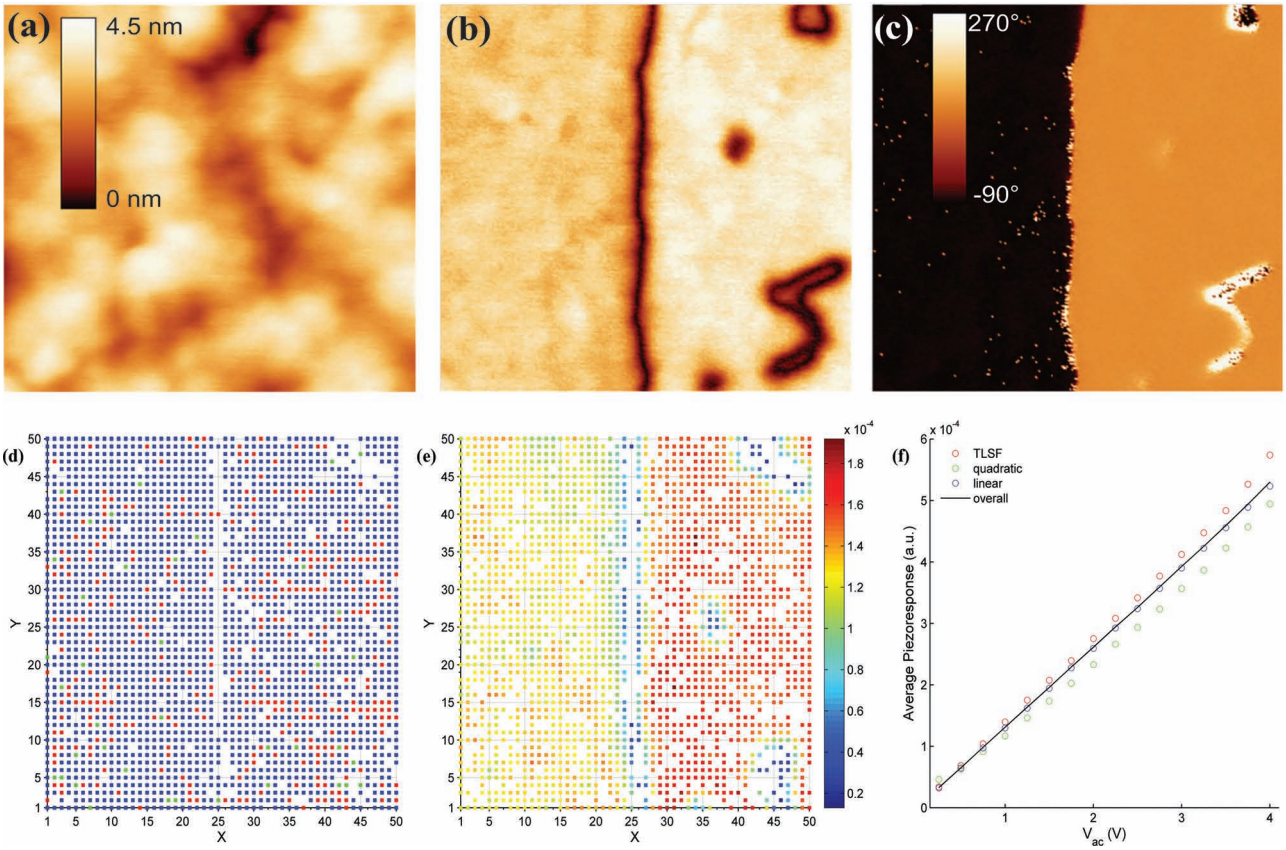

Figure 5. Probing the role of 180° wall motion. a) 1 μm × 1 μm topography. b) Vertical PFM amplitude and associated c) vertical PFM phase image of a written 180° domain wall. A band-excitation piezoresponse study was performed in this region. The response was mostly linear across the sample, as shown in the fitting map in (d) (the color scheme is the same as that used in Figure 2a). Of the 2303 points shown, 84.2% are linear, 1.7% is quadratic and 14.1% are TLS. e) A map of the linear coefficient α_1 shows the contrast decreases in the vicinity of the ferroelectric domain wall. The average piezoresponse in the studied region is plotted in (f).

ii) 200 nm-thick PZT film

$$d_{\text{eff}} = 4.714\times 10^{-5} + 1.456\times 10^{-6}\times V_{\text{ac}} \rightarrow (V_{\text{ac}} < 3.1\text{V}) \quad (6)$$

In analogy with the strain-electric field Rayleigh loops,[39] here we give a similar relation between the overall average piezoresponse, P_{ave}, and V_{ac} employing the d_0 and α_{d} parameters as

$$P_{\text{ave}} = \left(d_0 + \alpha_{\text{d}} V_{\text{ac}}^{\max}\right) V_{\text{ac}} \pm \frac{\alpha_{\text{d}}}{2}\left[\left(V_{\text{ac}}^{\max}\right)^2 - \left(V_{\text{ac}}\right)^2\right] \quad (7)$$

where $V^{\max}{}_{\text{ac}}$ is the maximum (amplitude of the) probing AC voltage. The – and + signs refer to the branches of the loop on which V_{ac} monotonously increases and decreases, respectively, between $\pm V^{\max}{}_{ac}$. The expected hysteresis loops from Equation (7) for a series of $V^{\max}{}_{\text{ac}}$ along with their corresponding P_{ave} values (horizontal dotted lines) from Figure 4b are shown in Figure 4e for the 2μm-thick PZT film (plots for the 200 nm-thick PZT film are provided in Supporting Information S6). It seems the P_{ave} at the tip of the loops $V_{\text{ac}} = V^{\max}{}_{\text{ac}}$ is underestimated in the 1st Rayleigh region and overestimated in the 2nd region. A confirmation of such a phenomenon would require investigation of minor hysteresis loops and nonlinearity at the nanoscale concurrently, which remains ongoing. However, we simply emphasize here that the key features of the Rayleigh law are recoverable when TLS behaviors are spatially averaged over larger length scales.

In order to decouple the piezoelectric coefficient contributions from ferroelectric and ferroelastic wall motion, measurements were performed on a PZT sample of same composition (thickness 200 nm) that is c-axis oriented, i.e., exhibits only c-domains. A 180° wall was created by biasing the tip at +10 V and scanning across the sample, and subsequently scanning over half the pre-poled area, as shown in the topography, vertical PFM amplitude and associated phase images in **Figure 5**a–c. An AC-dependent piezoresponse study (range 0.25 to 4V_{ac}) was then performed in this region. The fitting map is shown in Figure 5d, with the majority of the map colored blue, indicating purely linear fits to the data (the color scheme is the same as used in Figure 2a). Some points show double-linear behavior, which are marked red. The ferroelectric wall itself provides no response and is thus white. The α_1 map for this sample (i.e., the linear coefficient at each point) is drawn in Figure 5e. The average piezoresponse across the sample, for the three different

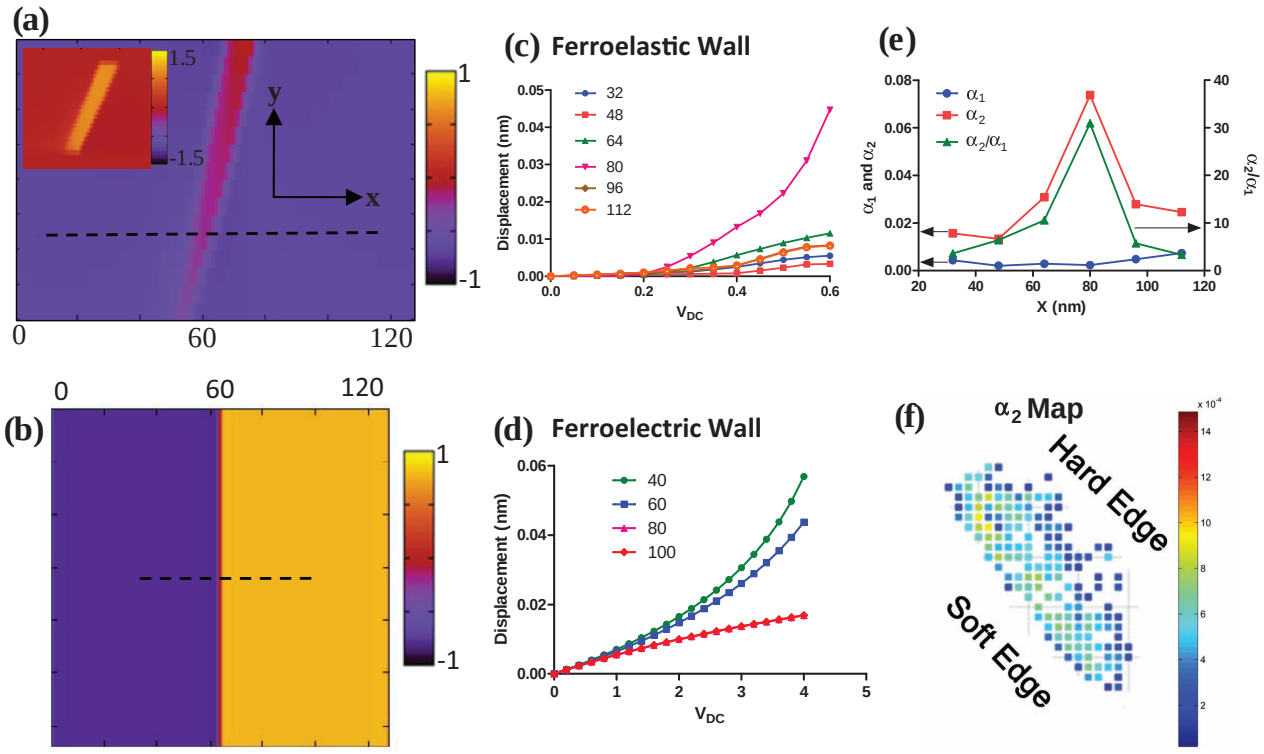

Figure 6. Phase-field modeling of behavior of ferroelectric and ferroelastic wall under applied fields. Shown in (a) is z-surface (i.e., *x*-*y* plane of polarization P_3) of a simulated c/a/c ferroelastic domain structure (the *x*-*z* plane is inset, showing P_2 and the direction of wall tilt). Similarly, a simulated ferroelectric (180°) wall is shown below in (b) (*z*-surface, polarization map P_3). The tip was then placed at various points along the dotted lines in (a) and (b) and the local surface displacement was calculated as a function of (DC) bias. The individual response curves for points along the dotted lines are graphed in (c) and (d) for both domain wall types. From the calculated ferroelastic wall responses, we applied our phenomenological model and calculated α_1, α_2 and the ratio α_2/α_1 for each point. The line profiles calculated for the ferroelastic wall in this way are shown in (e). A spatial map of α_2 from a single c-domain in the thick PZT sample, with the soft and hard edges marked, is shown in (f) for comparison.

types of responses, is plotted in Figure 5f. The average is well described by a purely linear equation. We note here that it has been found that even the motion of a ferroelectric wall can increase the piezoelectric coefficient, and result in a strain-ac electric field amplitude nonlinearity, providing the applied field drives a nearly reversible poling/de-poling process, which has been termed the "dynamic poling" model.[27–29] In our case, it may be that the ferroelectric domain wall is heavily clamped, and thus the response is purely intrinsic. Alternatively, the contribution from such a mechanism may be small enough to make detection difficult, especially since it is expected to contribute to mainly through a second-order harmonic in the strain.[28]

To better quantify the link between the enhanced d_{33} and motion of individual domain walls, phase-field modeling was performed (Supporting Information S7). We specifically explore evolution of wall deformation and twist[40] with applied bias, and define the numerical measures of the wall deformation as:

$$\text{Wall Deformation} = \int (P_{IP,E=xV} - P_{IP,E=0V})^2 \, dV \quad (8)$$

where P_{IP} is the magnitude of the in-plane polarization i.e., $(P_x^2 + P_y^2)^{1/2}$. The wall deformation is thus a measure of the twist of the polarization as a result of applying x volts (DC) through the tip. Note the integration is performed over a small local region (volume), which is approximated as x^3. We further model the surface displacement, u_3 which emulates the PFM signal. We modeled a single ferroelectric and a single ferroelastic wall, which are shown in **Figure 6**a,b (the side-view of the ferroelastic wall is shown inset, to illustrate the wall tilting direction). Shown in Figure 6c,d is displacement vs. bias along different points on the dotted lines in Figure 6a,b for both types of walls. First, it is immediately apparent that the modeling shows ferroelectric displacements are far less than the for the ferroelastic wall case, as in the experiment. Modeling confirms that the ferroelectric wall plays no role in assisting or hindering the surface displacement (note here that the reason for reduced response near the wall is because the displacements are for DC bias, and are thus affected by the domain's polarization orientation). For the ferroelastic case, however, there is significant enhancement of surface displacement as the ferroelastic wall is approached. There is also significant asymmetry, with the response peaking on the right side of the wall. We note that the peaking is on the "soft" side of the ferroelastic wall, remarkably similar to experiment (Figure 2g).

For the ferroelastic case, we fit this dependence of the displacement on the distance to the domain wall using the same phenomenological function as experiment and plot the extracted α_1,α_2 and α_2/α_1 across the domain wall, as shown in Figure 6e. Clearly, the ratio rises as the domain wall is approached (at $x = 60$),

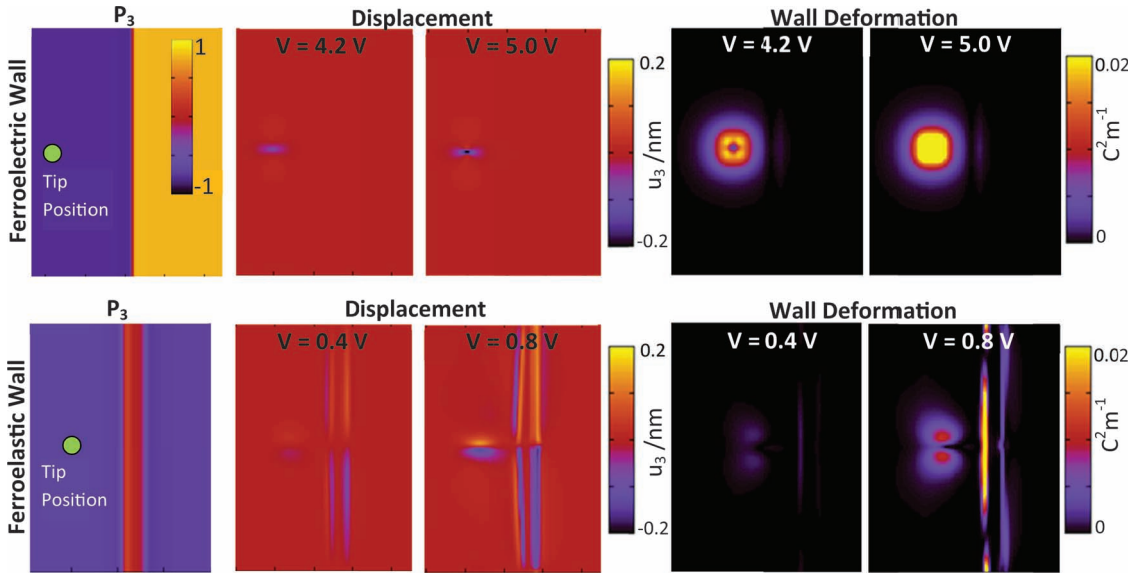

Figure 7. The role of wall twist in affecting surface displacement. To determine the role of domain wall twist in enhancing piezoresponse, the *z*-surface displacement and wall deformation maps were calculated for the ferroelectric (1st row) and ferroelastic (2nd row) cases, which are shown as a panel figure for two different sub-coercive voltages. The location of the tip in each case is indicated by the green circle on the P_3 polarization map on the left. In both cases the distance to the wall was ≈20 nm.

as we see in experiment. Furthermore, α_2 peaks near the soft edge (i.e., at $x = 80$). For comparison, the spatial variation of α_2 for a single c-domain is drawn in Figure 6f, which again shows agreement with the phase-field simulation. The (qualitative) similarity between the modeling and the experiment verifies that phase-field simulations can be utilized in determining the effect of domain dynamics on observed (AC) piezoresponse.

Having verified that the model reproduces our experimental observations, we attempt to gain insight into mechanisms, and specifically, the contribution of the wall deformation on the surface displacement. Shown in **Figure 7** are displacement and "wall deformation" surface plots, when the tip is placed near a ferroelectric (upper panel) and ferroelastic (lower panel) wall for differing DC bias. The position of the tip is indicated by the green circles. It can be seen that in the sub-coercive region the wall deformation behavior for the ferroelectric wall and ferroelastic exhibit different character. The wall deformation for ferroelectric wall with mid-range bias (4 V) is extremely small, while that of the ferroelastic wall are significant enough to be observed even for small bias (0.6 V). This reflects the increased interaction between the tip-field and the ferroelastic wall, leading to significant domain wall twist. In contrast, the ferroelectric wall does not appear to interact with the tip-field. Electrostatic energy analysis (Supporting Information S8) reveals that the 90° domain wall is less stable compared to the 180° domain wall, thus facilitating a twisting wall motion at much lower bias. The energy analysis also reveals the reason for the asymmetric response found on either side of the a/c domain boundary. An energetically active (with respect to electrostatic interactions) region exists near the "soft" (right) side, which would facilitate domain motion under applied fields. In contrast, the "hard" (left) side corresponds to a low energy regime which is largely inactive. The existence of these two regions appears to be due to elastic considerations: elastic energy distribution maps (Supporting Information S8) show that stress is largely relieved on the left side of the wall. In contrast a larger fraction of the c-domain on the right side is under higher compressive stress, leading to higher electrostatic and elastic energies, and hence an increased propensity to become perturbed under applied fields. By contrast, the energy regions of the ferroelectric wall are stable except for the sharp region at the domain wall. These phase-field simulations reveal that the motion of the ferroelastic wall is likely a twisting one, and dramatically enhance the electromechanical response of the system.

3. Conclusions

In summary, we undertook a bottom-up approach, i.e., locally determined piezoresponse behaviors are assembled together to yield a piezoresponse on a macroscale which is in agreement with the Rayleigh law, complementing the top-down approaches followed to-date relying on macroscopic measurements to infer nanoscale response. These studies suggest that nanoscale piezoresponse measurements in ferroelastic films probe a distinctly non-Rayleigh regime. Here, the response as a function of applied voltage appears to be characterized by two linear regions, with differing slopes and a transition voltage V_c. We interpret the initial linear region as the reversible intrinsic (lattice) response, and the second linear region as the intrinsic response in addition to an extrinsic response from the irreversible motion of a ferroelastic domain wall. It is shown that an average of such behaviors can lead directly to the Rayleigh behavior at the macroscale, while likely maintains the links between hysteresis and nonlinearity typical of Rayleigh systems. In contrast, studies of films with purely ferroelectric walls show

only linear response. Phase-field modeling suggests the source of the enhancement of the piezoresponse at the nanoscale, for ferroelastic walls, is a twisting motion induced by the applied field. These studies shed light on nonlinear Rayleigh behaviors in disordered ferroics.

4. Experimental Section

Band-excitation piezoresponse force microscopy was used in order to determine the piezoresponse as a function of AC bias across an array of points for three separate films. More details on the technique are available elsewhere.[23] The three films were: 1) 2 μm-thick $PbZr_{0.44}Ti_{0.56}O_3$ grown on (100) Si, 2) 200 nm-thick $PbZr_{0.44}Ti_{0.56}O_3$, grown on (100) $SrTiO_3$, and 3) 200 nm-thick $PbZr_{0.44}Ti_{0.56}O_3$ grown on (100) CaF_2. All films were grown using pulsed laser deposition. Each film was deposited on a layer of $SrRuO_3$ to act as the electrode for PFM and switching experiments. The sample was then studied using a commercially available scanning probe microscope (Asylum Research, Cypher model) equipped with NI PXI based band excitation controller to enable band-excitation (BE) measurements, with the data analyzed using MATLAB software (v7). The response at each point was captured across the frequency band centered on the resonant frequency of the cantilever. This was then fit to a simple harmonic oscillator model to yield the piezoresponse amplitude, phase, the Q-factor and the resonance at each voltage step. Image processing was carried out using WSxM v5.0[41], and some graphs were made using GraphPad Prism v5.03. Details of phase-field simulations can be found in the Supporting Information.

Supporting Information

Supporting Information is available from the Wiley Online Library or from the author.

Acknowledgements

R.K.V. and M.B.O. contributed equally to this work. The authors acknowledge fruitful discussions with D. Damjanovic and J. Jones. R.K.V., M.B.O., and V.N. acknowledge support from the ARC Discovery Project scheme. R.K.V. and V.N. acknowledge an Overseas Travel Fellowship by the Australian Nanotechnology Network. The research at ORNL (A.K., S.J., S.V.K.) was conducted at the Center for Nanophase Materials Sciences, which is sponsored at Oak Ridge National Laboratory by the Division of Scientific User Facilities, U.S. Department of Energy. C.D. and L.Q.C are supported by the National Science Foundation under DMR-0908718 and DMR-0820404.

Received: April 8, 2012
Revised: July 5, 2012
Published online: August 10, 2012

[1] J. F. Scott, C. A. Paz de Araujo, *Science* **1989**, *246*, 1400.
[2] A. K. Tagantsev, V. O. Sherman, K. F. Astafiev, J. Venkatesh, N. Setter, *J. Electroceram.* **2003**, *11*, 5.
[3] M. E. Lines, A. M. Glass, *Principles and Applications of Ferroelectrics and Related Materials*, Oxford University Press, Oxford **1977**.
[4] K. S. Novoselov, A. K. Geim, S. V. Dubonos, E. W. Hill, I. V. Grigorieva, *Nature* **2003**, *426*, 812.
[5] Y.-H. Shin, I. Grinberg, I. W. Chen, A. M. Rappe, *Nature* **2007**, *449*, 881.
[6] K. H. Fischer, J. A. Hertz, *Spin Glasses*, Cambridge University Press, Cambridge, UK **1991**.
[7] Z. Kutnjak, J. Petzelt, R. Blinc, *Nature* **2006**, *441*, 956.
[8] R. J. Zeches, M. D. Rossell, J. X. Zhang, A. J. Hatt, Q. He, C. H. Yang, A. Kumar, C. H. Wang, A. Melville, C. Adamo, G. Sheng, Y. H. Chu, J. F. Ihlefeld, R. Erni, C. Ederer, V. Gopalan, L. Q. Chen, D. G. Schlom, N. A. Spaldin, L. W. Martin, R. Ramesh, *Science* **2009**, *326*, 977.
[9] L. Rayleigh, *Philos. Mag. Series 5* **1887**, *23*, 225.
[10] L. Néel, *Cahiers Phys.* **1942**, *12*, 1.
[11] D. Damjanovic, *J. Appl. Phys.* **1997**, *82*, 1788.
[12] V. V. Shvartsman, N. A. Pertsev, J. M. Herrero, C. Zaldo, A. L. Kholkin, *J. Appl. Phys.* **2005**, *97*, 104105.
[13] T. Nattermann, *EPL* **1987**, *4*, 1241.
[14] T. Nattermann, Y. Shapir, I. Vilfan, *Phys. Rev. B* **1990**, *42*, 8577;
[15] T. Giamarchi, A. B. Kolton, A. Rosso, in *Jamming, yielding, and irreversible deformation in condensed matter*, Vol. *688* (Eds: M. C. Miguel, J. M. Rubí), Springer Verlag, Berlin **2006**.
[16] N. A. Pertsev, G. Arlt, A. G. Zembilgotov, *Microelectron. Eng.* **1995**, *29*, 135.
[17] N. A. Pertsev, A. Y. Emelyanov, *Appl. Phys. Lett.* **1997**, *71*, 3646.
[18] N. A. Pertsev, A. Y. Emelyanov, *Phys. Rev. B* **2002**, *65*, 174115.
[19] T. J. Yang, V. Gopalan, P. J. Swart, U. Mohideen, *Phys. Rev. Lett.* **1999**, *82*, 4106.
[20] P. Paruch, T. Giamarchi, J. M. Triscone, *Phys. Rev. Lett.* **2005**, *94*, 197601;
[21] G. Catalan, H. Bea, S. Fusil, M. Bibes, P. Paruch, A. Barthelemy, J. F. Scott, *Phys. Rev. Lett.* **2008**, *100*, 027602.
[22] J. Y. Jo, S. M. Yang, T. H. Kim, H. N. Lee, J. G. Yoon, S. Park, Y. Jo, M. H. Jung, T. W. Noh, *Phys. Rev. Lett.* **2009**, *102*, 045701.
[23] P. Bintachitt, S. Jesse, D. Damjanovic, Y. Han, I. M. Reaney, S. Trolier-McKinstry, S. V. Kalinin, *Proc. Natl. Acad. Sci. USA* **2010**, *107*, 7219.
[24] A. Pramanick, D. Damjanovic, J. E. Daniels, J. C. Nino, J. L. Jones, *J. Am. Ceram. Soc.* **2011**, *94*, 293.
[25] G. Tutuncu, D. Damjanovic, J. Chen, J. L. Jones, *Phys. Rev. Lett.* **2012**, *108*, 177601.
[26] J. Karthik, A. R. Damodaran, L. W. Martin, *Phys. Rev. Lett.* **2012**, *108*, 167601.
[27] S. Trolier-McKinstry, N. B. Gharb, D. Damjanovic, *Appl. Phys. Lett.* **2006**, *88*, 202901.
[28] N. Bassiri-Gharb, S. Trolier-McKinstry, D. Damjanovic, *J. Appl. Phys.* **2011**, *110*, 124104.
[29] N. B. Gharb, S. Trolier-McKinstry, D. Damjanovic, *J. Appl. Phys.* **2006**, *100*, 044107.
[30] S. Jesse, S. V. Kalinin, R. Proksch, A.P.Baddorf, B. J. Rodriguez, *Nanotechnology* **2007**, *18*, 435503.
[31] D. A. Hall, P. J. Stevenson, *Ferroelectrics* **1999**, *228*, 139.
[32] K. Lee, S. Baik, *Annu. Rev. Mater. Res.* **2006**, *36*, 81.
[33] C. S. Ganpule, V. Nagarajan, H. Li, A. S. Ogale, D. E. Steinhauer, S. Aggarwal, E. Williams, R. Ramesh, P. De Wolf, *Appl. Phys. Lett.* **2000**, *77*, 292.
[34] B. J. Rodriguez, S. Jesse, K. Seal, N. Balke, S. V. Kalinin, R. Proksch, in *Scanning Probe Microscopy of Functional Materials*, (Eds: S. V. Kalinin, A. Gruverman), Springer, New York **2010**, 491.
[35] V. Nagarajan, A. Stanishevsky, L. Chen, T. Zhao, B. T. Liu, J. Melngailis, A. L. Roytburd, R. Ramesh, J. Finder, Z. Yu, R. Droopad, K. Eisenbeiser, *Appl. Phys. Lett.* **2002**, *81*, 4215.
[36] F. Xu, F. Chu, S. Trolier-McKinstry, *J. Appl. Phys.* **1999**, *86*, 588.
[37] F. Griggio, *Appl. Phys. Lett.* **2011**, *98*, 212901.
[38] G. Catalan, A. Lubk, A. H. G. Vlooswijk, E. Snoeck, C. Magen, A. Janssens, G. Rispens, G. Rijnders, D. H. A. Blank, B. Noheda, *Nat. Mater.* **2011**, *10*, 963.
[39] A. Pramanick, D. Damjanovic, J. C. Nino, J. L. Jones, *J. Am. Ceram. Soc.* **2009**, *92*, 2291.
[40] N. Balke, S. Choudhury, S. Jesse, M. Huijben, Y. H. Chu, A. P. Baddorf, L. Q. Chen, R. Ramesh, S. V. Kalinin, *Nat. Nanotechnol.* **2009**, *4*, 868.
[41] I. Horcas, R. Fernandez, J. M. Gomez-Rodriguez, J. Colchero, J. Gomez-Herrero, A. M. Baro, *Rev. Sci. Instrum.* **2007**, *78*, 013705.